2017

Multiangular Rod-Shaped Na0.44MnO2 as Cathode Materials with High Rate and Long Life for Sodium-Ion Batteries

Qiannan Liu
University of Wollongong, ql953@uowmail.edu.au

Zhe Hu
University of Wollongong, zh865@uowmail.edu.au

Mingzhe Chen
University of Wollongong, mc800@uowmail.edu.au

Qinfen Gu
Australian Synchrotron Company

Yuhai Dou
University of Wollongong

See next page for additional authors

Publication Details

Liu, Q., Hu, Z., Chen, M., Gu, Q., Dou, Y., Sun, Z., Chou, S. & Dou, S. Xue. (2017). Multiangular Rod-Shaped Na0.44MnO2 as Cathode Materials with High Rate and Long Life for Sodium-Ion Batteries. ACS Applied Materials and Interfaces, 9 (4), 3644-3652.

Multiangular Rod-Shaped Na0.44MnO2 as Cathode Materials with High Rate and Long Life for Sodium-Ion Batteries

Abstract

The tunnel-structured Na0.44MnO2 is considered as a promising cathode material for sodium-ion batteries because of its unique three-dimensional crystal structure. Multiangular rod-shaped Na0.44MnO2 have been first synthesized via a reverse microemulsion method and investigated as high-rate and long-life cathode materials for Na-ion batteries. The microstructure and composition of prepared Na0.44MnO2 is highly related to the sintering temperature. This structure with suitable size increases the contact area between the material and the electrolyte and guarantees fast sodium-ion diffusion. The rods prepared at 850 °C maintain specific capacity of 72.8 mA h g−1 and capacity retention of 99.6% after 2000 cycles at a high current density of 1000 mA g−1 . The as-designed multiangular Na0.44MnO2 provides new insight into the development of tunnel-type electrode materials and their application in rechargeable sodiumion batteries

Disciplines

Engineering | Physical Sciences and Mathematics

Publication Details

Liu, Q., Hu, Z., Chen, M., Gu, Q., Dou, Y., Sun, Z., Chou, S. & Dou, S. Xue. (2017). Multiangular Rod-Shaped Na0.44MnO2 as Cathode Materials with High Rate and Long Life for Sodium-Ion Batteries. ACS Applied Materials and Interfaces, 9 (4), 3644-3652.

Authors

Qiannan Liu, Zhe Hu, Mingzhe Chen, Qinfen Gu, Yuhai Dou, Ziqi Sun, Shulei Chou, and Shi Xue Dou

Multi-angular Rod-Shape $Na_{0.44}MnO_2$ as Cathode Materials with High-Rate and Long-Life for Sodium-Ion Batteries

Qiannan Liu,[†] Zhe Hu,[†] Mingzhe Chen,[†] Qinfen Gu,[*, ‡] Yuhai Dou,[†] Ziqi Sun,[*, §] Shulei Chou,[*, †] and Shi Xue Dou[†]

[†] Institute for Superconducting and Electronic Materials, Australian Institute for Innovative Materials, University of Wollongong, Innovation Campus, Squires Way, North Wollongong, NSW 2522, Australia

[‡] Australian Synchrotron, 800 Blackburn Rd, Clayton, VIC 3168, Australia

[§] School of Chemistry, Physics and Mechanical Engineering, Queensland University of Technology, Gardens Point, Brisbane, QLD 4000, Australia

KEYWORDS: multi-angular $Na_{0.44}MnO_2$, high-rate, long life, cathode, sodium ion batteries

ABSTRACT: The tunnel-structured $Na_{0.44}MnO_2$ is considered as a promising cathode material for sodium ion batteries due to its unique three-dimensional (3D) crystal structure. Multi-angular rod-shape $Na_{0.44}MnO_2$ have been firstly synthesized via a reverse microemulsion method and investigated as high-rate and long-life cathode materials for Na-ion batteries. The microstructure and composition of prepared $Na_{0.44}MnO_2$ is highly related to the sintering temperature. This structure with suitable size increases the contact area between the material and the electrolyte and guarantees fast sodium ion diffusion. The rods prepared at 850℃ maintain specific capacity of 72.8 mAh g^{-1} and capacity retention of 99.6% after 2000 cycles at a high current density of 1000 mA g^{-1}. The as-designed multi-angular $Na_{0.44}MnO_2$

provides new insight into the development of tunnel-type electrode materials and their application in rechargeable sodium-ion batteries.

1. INTRODUTION

The demand for large-scale energy storage devices has been growing significantly due to the continuous depletion of energy resources.[1] Sodium ion batteries (SIBs), a new generation of large-scale rechargeable energy storage devices, are attracting more and more attention because of the low cost and abundant availability of sodium resources. Nevertheless, the sluggish electrochemical reaction kinetics resulting from the large diameter of the Na^+ ion makes it very difficult to find suitable host materials for rapid and reversible Na^+ insertion and extraction.[2-4] Therefore, it is highly desirable to develop effective Na-host materials for high performance SIBs with high specific capacity, high rate capability, and long-term cycling stability.[2-8]

Considering the cost factor, the sodium manganese oxides (Na_xMnO_2), such as $NaMnO_2$, $Na_{0.60}MnO_2$ and $Na_{0.44}MnO_2$, have been studied as promising cathode materials for SIBs since they were reported by Parant *et al.* in 1971.[9] For Na_xMnO_2, a tunnel-type structure is formed at $0.22 \leq x \leq 0.44$, a mixture of tunnel and layered structures is formed at $0.44 < x \leq 0.66$, and a fully layered structure is formed at $0.66 < x \leq 1$.[10] Among these structures, the tunnel-structured $Na_{0.44}MnO_2$ is particularly attractive due to its unique three-dimensional (3D) crystal structure, which is made up of MnO_5 pyramids and MnO_6 octahedra, and is able to

tolerate some stress during structural change.[10-15] $Na_{0.44}MnO_2$, with a theoretical discharge capacity of 121 mAh g^{-1} (1 C = 121 mA g^{-1}), has a framework containing large S tunnels and small tunnels, and among them, the S tunnels can provide an abundance of vacancies, where 0.22 Na^+ can be reversibly extracted along the *c*-axis.[16-18] The crystal structure of $Na_{0.44}MnO_2$ is shown in Figure S1 in the supporting information. It is difficult, however, for the $Na_{0.44}MnO_2$ lattice to well accommodate the structural changes during the insertion/extraction of Na^+, leading to poor rate capability, which severely restricts its practical applications. Sauvage e*t al.* prepared $Na_{0.44}MnO_2$ with an initial capacity of 80 mAh g^{-1} at 0.1 C.[19] The capacity faded rapidly, however, with only half of the initial capacity retained after 50 cycles. Many strategies, such as nanosizing and metal substitution, have been tried to alleviate this disadvantage. Cao *et al.* reported $Na_{0.44}MnO_2$ nanowires with a discharge capacity of 84.2 mAh g^{-1} over 1000 cycles at 0.5 C.[20] Wang *et al.* prepared Ti-substituted $Na_{0.44}MnO_2$ with capacity retention higher than 96% after 1100 cycles at 0.1 C.[21] There is no report, to the best of our knowledge, on $Na_{0.44}MnO_2$ with both excellent high-rate (more than 5 C) capacity and long cycling life for sodium storage.

$Na_{0.44}MnO_2$ can be prepared *via* facile synthetic methods such as hydrothermal,[22] solid-state,[19] sol-gel,[23] polymer-pyrolysis,[6] and reverse microemulsion method[16] *etc*. The preparation methods and electrochemical performance of the $Na_{0.44}MnO_2$ as cathode for SIBs are summarized in **Table 1**. The products obtained by different methods display different

electrochemical performance. Among those methods, the reverse microemulsion process involves thoroughly dispersing a water phase into an oil phase consisting of a surfactant and a co-surfactant, to form thermodynamically stable microemulsion droplets (reverse micelles), in which each droplet acts as an independent microreactor to help produce the desired compound.[24] It can help to synthesize small particles with a narrow size distribution.[25]

In this work, we have prepared monophasic $Na_{0.44}MnO_2$ with multi-angular shaped rods by a modified reverse microemulsion method.[16] To the best of our knowledge, this is the first time that $Na_{0.44}MnO_2$ with multi-angular images has been reported. This structure with suitable size increases the contact area between the material and the electrolyte, guarantees fast sodium ion diffusion and helps release strains resulting from de-insertion/insertion of Na^+ ions in multiple directions. When used as cathode material in SIBs, the as-prepared multi-angular $Na_{0.44}MnO_2$ rods feature stable cycling performance, excellent high-rate capability, and long cycle life at 8.3 C.

2. EXPERIMENTAL SECTION

Material Preparation. Multi-angular rod-shaped $Na_{0.44}MnO_2$ was synthesized through a reverse microemulsion method. All the chemicals were used as purchased. Sodium nitrate and manganese nitrate tetrahydrate with a Na/Mn ratio of 0.44 were dissolved successively in 9 mL deionized water to form the water phase. 0.2 g polyethylene oxide-polypropylene oxide-polyethylene oxide (PEO20-PPO70-PEO20, Pluronic P123, surfactant) was dissolved in 3 g

absolute ethanol with 20 mL ethylene glycol (EG, cosurfactant) added later to form the oil phase. After stirring for 30 minutes, the water phase was gradually dropped into the oil phase under continuous stirring. Then, the obtained microemulsion was heated at 80°C to vaporize the water. The obtained gel precursor was then heated in a muffle furnace at 700°C (NMO700), 750°C (NMO750), 800°C (NMO800), 850°C (NMO850), or 900°C (NMO900) for 20 h in air to obtain the final products.

Structural Characterization. The morphologies of the as-prepared samples were investigated by field-emission scanning electron microscopy (FESEM, JEOL JSM-7500) and transmission electron microscopy (TEM, JEOL ARM 200F). TEM samples were prepared after sonication treatment. The microstructures of the as-prepared powders were characterized on a synchrotron X-ray diffraction beamline with a wavelength (λ) of 0.6885 Å calibrated with the National Institute of Standards and Technology (NIST) LaB_6 660b standard reference material and laboratory X-ray diffraction (XRD, GBC MMA diffractometer) with Cu K_α radiation. The thermal property of the precursor before calcination was characterized by a Mettler−Toledo thermogravimetric analysis/differential scanning calorimetry (TGA/DSC) STARe System under air over a temperature range of 40–1000 °C with a ramp rate of 5°C min^{-1}.

Electrochemical Measurements. The electrodes were prepared by mixing 80 wt% active materials, 10 wt% Super P, and 10 wt% polyvinylidene fluoride (PVDF) binder to form a

slurry, which was then coated on an aluminium foil. Next, the aluminium foil was dried in a vacuum oven overnight at 120°C. After that, the working electrodes were cut out and pressed under a pressure of 20 MPa. The electrolyte used was 1.0 mol L^{-1} $NaClO_4$ in an ethylene carbonate (EC) – diethyl carbonate (DEC) solution (1:1 v/v) with 5 vol.% of fluoroethylene carbonate (FEC). Sodium foil was cut from a sodium bulk stored in mineral oil and used as both the counter and reference electrode. The cells were assembled in an argon-filled glove box. The electrochemical performances were tested on a Land Test System in the voltage range of 3.8-2.0 V (vs. Na^+/Na) at different current densities. Cyclic voltammetry (CV) at a scan rate of 0.1 mV s^{-1} and electrochemical impedance spectroscopy (EIS) from 100 kHz to 100 mHz were performed using a CHI 660b electrochemistry workstation between 4.0-2.0 V. In situ synchrotron XRD data were collected at the Australian Synchrotron with a wavelength (λ) of 0.6885 Å, calibrated with the NIST LaB_6 660b standard reference material. The cell used was charged at a current density of 12.1 mA g^{-1} (0.1 C), and the cutoff voltage was 3.8-2.0 V. The diffusion coefficient of Na^+ ions was studied using the galvanostatic intermittent titration technique (GITT) and EIS. For the GITT measurement, the cells were charged and discharged at 0.1 C for 360 s followed by an open circuit relaxation for 1 h. The procedure was maintained until the voltage reached 3.8 V or 2.0 V. All the electrochemical testings were conducted at room temperature.

3. RESULTS AND DISCUSSION

The shape-defined cathode material, $Na_{0.44}MnO_2$, was synthesized via a reverse microemulsion method from the mixed solution of P123, EG, ethanol and water. A gel precursor was formed after removing the water from the precursor solution by heating at 80°C, and then the targeted material could be obtained by further heating the precursor at a higher temperature in air. The TGA/DSC test was employed to study the chemical reactions and crystallization behaviours of the gel precursor during calcination. **Figure 1**a is the TGA curve of the gel precursor between 40 and 1000°C. Two distinct weight losses were observed during heated to 370°C (Zone 1 and Zone 2), which can be attributed to the removal of remnant water and ethylene glycol, respectively. Further heating to 1000°C, as shown in the magnified image of Zone 3 (~1% weight loss), slight weight variations occurred at around 750°C and 850°C were monitored. Figure 1b presents synchrotron XRD spectra of the powders calcined at different temperatures, which indicates the change on the compositions and crystal structures of the products after heating. At 700°C, $Na_{0.44}MnO_2$ ($Na_4Mn_9O_{18}$) together with $Na_{0.4}MnO_2$ ($Na_2Mn_5O_{10}$) was obtained due to a slight loss of Na during the preparation process. It was reported that the psilomelane $Na_{0.4}MnO_2$ decomposes at temperatures above 750°C based on the equation below:[9]

$$0.44\ Na_{0.4}MnO_2 \rightarrow 0.40\ Na_{0.44}MnO_2 + 0.02\ Mn_2O_3 + 0.01O_2 \uparrow \quad (1)$$

which caused a small change in the weight loss at 750°C in the TGA curve. There were still $Na_{0.4}MnO_2$ residues detected for NMO800. Another phase transformation took place from

800 to 850°C, and the $Na_{0.4}MnO_2$ phase almost disappeared in NMO850. Meanwhile, traces of unknown phases were detected in NMO850 and became less in NMO900. Those transformations are in accordance with the change in the weight loss at and after 850°C in the TGA curve. No other phases apart from $Na_4Mn_9O_{18}$ and $Na_2Mn_5O_{10}$ could be detected in the XRD patterns shown in Figure S2, indicating that the content of impurities was less than 5 mol%. All the $Na_{0.44}MnO_2$ peaks can be indexed to the orthorhombic phase with space group Pbam (JCPDS No. 27-750, a = 9.100 Å, b = 26.340 Å, and c = 2.821 Å). The intensities of the $Na_{0.44}MnO_2$ peaks become stronger with increasing temperature, indicating the better crystallinity and larger crystallite size of the sample. The (3 5 0) reflection of all the $Na_{0.44}MnO_2$ samples split into two Bragg peaks for (0 10 0) and (3 5 0) with changing relative intensity for samples calcined at different temperatures in both patterns. Rietveld refinement was performed on the synchrotron XRD pattern collected from NMO850 as a single phse,[13, 26] and is shown in Figure S3. The structural formula is fitted to $Na_{4.34}Mn_9O_{18}$, indicating more sodium existing in the composite than $Na_4Mn_9O_{18}$. Since the impurity phase is very little, we can not get the exact phase through the Rietveld refinment.

The morphologies of samples calcined at different temperatures are shown in **Figure 2**. All the samples presented well-distributed multi-angular rod-shape morphology with grooves on the surfaces. It can be seen that the rods of NMO750 were well-isolated with diameters in the range of 0.1-0.5 μm and lengths of 0.5-2.5 μm. With increasing sintering temperature, the

rods become bigger and longer and the grooves become more obvious. This growth is consistent with the increasing intensity of the XRD results. The multi-angular rods tend to fuse together to decrease the surface energy at 850 and 900°C. The edges of the grooves tend to be deeper and sharper for NMO850 but smoothened when calcined at 900°C.

To understand the effects of P123 and EG, we prepared samples without the addition of P123 or EG, while the other conditions were maintained as the same with NMO850. The XRD patterns and SEM morphologies of the samples obtained without the addition of P123 or EG are shown in Figure S4 and Figure S5, respectively. It can be clearly seen that the rods obtained from the solution without P123 formed with manganese oxide impurities, and are shorter and thicker comparing with those prepared with the addition of P123 as shown in Figure 2c. The grooves on the surfaces are far less obvious than those in Figure 2c, which may result from the lack of morphology controlling effect of surfactant P123 to form shape-defined grooves.[27] Moreover, without the addition of EG, the multi-angular rods are $Na_{0.44}MnO_2$ with Mn_2O_3 impurities, the content of which is much larger than 5 mol%, as shown in Figure S4. The rods are longer and thinner than those shown in Figure 2c and Figure S5a and S5b. EG helps to inhibit the formation of superabundant Mn_2O_3. Therefore, the addition of P123 and EG is essential for synthesizing pure-phase multi-angular $Na_{0.44}MnO_2$ product.

TEM investigations were also carried out to study the microstructures of samples calcined at different temperatures, as shown in **Figure 3**. It can be seen that the diameter is ~ 0.5 μm of one single rod for all samples. The image contrast observed on the rods in the TEM images and the corresponding high-resolution TEM images (HRTEM) is ascribed to the variations in the thickness of the samples resulting from the grooves on the surface. The rods of NMO850 and NMO900 tightly fused together and remained adhesive after sonication, as shown in Figure 3b and 3c, which are consistent with the SEM results. All the rods calcined at different temperatures show clear lattices in the HRTEM images (Figure 3d-3f). All of the lattice fringes have a spacing of 0.455 nm, corresponding to the (200) planes of $Na_{0.44}MnO_2$. The selected area electron diffraction (SAED) pattern (inset of Figure 3e) of NMO850 reveals that the rods are single-crystalline $Na_{0.44}MnO_2$ with orientation along the [001] direction, which is consistent with other reports.[28, 29] The impurity content is too low to be detected. Similar SAED patterns also exist for NMO800 and NMO900 (not shown).

The $\vec{c}$ ([001]) direction, along which a $Na_{0.44}MnO_2$ crystal grows much faster than in other directions, is the main path for sodium diffusion of $Na_{0.44}MnO_2$.[30, 31] Therefore, $Na_{0.44}MnO_2$ tends to grow into rod- or wire-like shapes, as summarized in Table 1. To the best of our knowledge, this is the first time that multi-angular $Na_{0.44}MnO_2$ rods are reported. The multi-angular structure is theoretically favourable for materials intended as electrodes for batteries. In this case, it can not only increase the contact area between the $Na_{0.44}MnO_2$ rods and the

electrolyte, but also accelerate the diffusion of sodium ions in the bulk of the material. The aligned grooves on the surface of the 1D rods can endorse the material enhanced wettability and directional diffusion of the electrolyte along the grooves.[32] Also, the multi-angular structure can help release strains resulting from de-insertion/insertion of Na^+ ions in multiple directions. The relatively large particle size is also good to improve the volumetric energy density.

NMO850 and NMO900 were chosen for further electrochemical testing since they are mainly composed of $Na_{0.44}MnO_2$ without $Na_{0.4}MnO_2$. **Figure 4**a shows CV curves of NMO850 and NMO900. For NMO850, the voltage peaks in the oxidation process for the initial cycle were centred at 3.09, 3.31, and 3.51 V, respectively. The cathodic scan shows six peaks at 3.37, 3.13, 2.93, 2.61, 2.36, and 2.15 V, which is consistent with the reported six biphasic transitions, implying a complex multiphase transition mechanism during Na-ion insertion and extraction processes.[19, 20] Six highly reproducible redox processes can be clearly seen in the following cycles, as shown in Figure S6. There is little difference between the first cycle and the subsequent cycles, demonstrating the stable charge and discharge processes. This result is different from some other reports, in which the initial anodic scans are stronger than those in the subsequent cycles.[12, 15] This can be attributed to the strain tolerance of the multi-angular structure for Na^+ de-insertion/insertion. It can be seen that the CV curves of NMO900 shows similar transitions and same position of reduction peaks compared with

NMO850. The voltage peaks in the oxidation process, however, exhibit values higher than those of NMO850 and were observed at 3.13, 3.34, and 3.54 V respectively, indicating its more serious polarization. This may be responsible for the difference in the discharge capacity between them.

The charge-discharge curves (Figure 4b) of NMO850 and NMO900 at 0.1 C also display six plateaus, which are consistent with the CV results and could be attributed to the extraction of Na^+ from different sites.[14, 33] It was reported that the Na ions located in the S-shape tunnels can produce a theoretical capacity of 50 mAh g^{-1}.[34] In our work, the initial charge capacity of NMO850 at 0.1 C is 49.4 mAh g^{-1}, corresponding to the extraction of 0.18 Na^+ from the $Na_{0.44}MnO_2$ framework.

The cycling performances of NMO850 and NMO900 were investigated at the high current density of 8.3 C, as shown in Figure 4c. It can be seen that both the samples exhibit a stable cycling performance with negligible decay within 1000 cycles. In detail, NMO850 and NMO900 deliver initial discharge capacities of 73.1 and 27.9 mAh g^{-1}, respectively. From the inset amplification image, it can be found that both the discharge capacity kept increasing during the first 200 cycles, arising from an activation process. The discharge capacities were 82.1 and 39.8 mAh g^{-1} after about 1000 cycles for NMO850 and NMO900, respecively. In particular, NMO850 retained a discharge capacity of 72.8 mAh g^{-1} after 2000 cycles, corresponding to a high capacity retention of 99.6% of the initial capacity. Moreover, the

coulombic efficiency was 212% in the first cycle and remained stable at nearly 100% up to 2000 cycles. The cycling performances of NMO850 and NMO900 at 0.1 C are shown in Figure S7. At both 8.3 C and 0.1 C, NMO850 exhibits high capacity and good cycling stability owing to its composition, unique morphology, and suitable particle size. NMO900, however, shows lower reversible specific capacity due to the greater strains resulting from its bigger particle size and smoother surface (Figure 2d and 3c). The capacity and stability related to the size of $Na_{0.44}MnO_2$ was also testified by Zhan *et al.*[16] and Cao *et al.*[20]

The rate capacities of NMO850 and NMO900 are shown in Figure 4d. It was observed that NMO850 retained specific capacities of 101.3, 95.1, 90.2, 84.8, 78.6, 68.8, and 54.7 mAh g^{-1} at 0.1, 0.2, 0.5, 1, 2, 5, and 10 C, respectively, and it can return back to 97.1 mAh g^{-1} at 0.1 C after cycling at 10 C. By contrast, NMO900 delivered much lower capacities. The good cycling and rate performance of NMO850 can also be ascribed to the well-defined 3D channel structure of the $Na_{0.44}MnO_2$, which effectively facilitates the extraction/ insertion of Na^+ ions. To the best of our knowledge, this is the best cycling performance, with long cycle life and high cycling stability at a high current density of 8.3 C, compared with other reported results for $Na_{0.44}MnO_2$, as summarized in Table 1.

Figure 5 show the GITT curves for the first cycle at 0.1 C of Na/NMO850 and Na/NMO900 cell and the corresponding sodium ion diffusion coefficent (D_{Na+}). It can be calculated that the D_{Na+} values of electrodes are between 4.9×10^{-16} and 2.15×10^{-14} cm^2 s^{-1}

for NMO850, and between 1.0×10^{-16} and 1.76×10^{-14} cm^2 s^{-1} for NMO900 in the range of 2.2 to 3.5 V, respectively. Meanwhile, the sodium ion diffusion coefficients of different electrodes were also investigated by electrochemical impedance spectroscopy at open circuit potential (OCP). The Nyquist curves and the corresponding Z_{re} vs. $\omega^{-1/2}$ plots in the low-frequency region are shown in Figure S8. The calculated D_{Na+} values are 2.40×10^{-14} and 1.90×10^{-14} cm^2 s^{-1} at the OCP for NMO850 and NMO900, respectively. The high D_{Na+} values well explain the excellent cycling performance of the $Na_{0.44}MnO_2$ multi-angualr rods. The D_{Na+} of NMO850 is larger than that of NMO900, indicating its faster sodium ion diffusion, which results from its more suitable size and more distinct multi-angular structure than those of NMO900.

In-situ X-ray synchrotron diffraction was also conducted to investigate the Na^+ de-insertion/insertion behaviour during the first charge-discharge process at 0.5 C for NMO850, as shown in **Figure 6**a. Potential drops are related to single-phase domains in a narrow sodium content range and the sloping curves are the signature of solid-solution behaviour.[27] There is no evident formation of new phases or superstructures but solid-solution reaction during the Na extraction/insertion from/into the $Na_{0.44}MnO_2$ framework.[35] It is clearly seen that all the peaks shift towards larger 2θ values during the charge process, indicating the extraction of Na^+ from and contraction of the unit cell in the $Na_{0.44}MnO_2$ framework. During the discharge process, those shifted peaks move back to lower degree and the phase can go

back to the original one (the same as the XRD of initial $Na_{0.44}MnO_2$) at ~2.8 V. The intensity of (200) decreased, especially after the phase recovered to the primary one (~2.8 V). Upon further discharging, the NMO framework kept expanding, which would cause the decrease of structure ordering, resulting in the decrease of peak intensity. At the end of discharge process, all the peaks shifted to lower degrees relative to the original ones, resulting from the insertion of more Na^+ into the $Na_{0.44}MnO_2$ framework during the discharge process than the extracted ones during the charge process. The two split peaks ((3 5 0) and (0 10 0)) around 34° merge into one peak when charged to 3.8 V, and the peak starts splitting again at the beginning of discharge. This could be caused by the changing amount of Na^+ ions in the structure due to the de-insertion/insertion of Na^+ ions.[36] The corresponding change of cell parameters *a*, *b*, *c* and volume are shown in Figure 6b. The parameters *a*, *b* and *c* all become smaller during the charge process due to extraction of Na^+ and turn to be larger during the discharge process. It can be seen that the charge process affects mainly the *b* parameter, while strong variation of *a* and *c* occur during the discharge process, in accordance with the changes in the (2 0 0) and (0 10 0) peaks in Figure 6a. Similar trends on the crystal structure parameters change have also been observed by Sauvage *et al*.[19] The volume change is calculated to be less than 2.53%, demonstrating the excellent structure stability and thus high cycling stability of this material during the charge and discharge processes.

To clarify the stability of the electrode, TEM characterization was performed on NMO850 electrode, which was discharged to 2.8 V after cycling for 100 times at 0.1 C. The same morphology of the bright field TEM image (**Figure 7**a) as for Figure 2c and Figure 3b demonstrates the stable structure of NMO850. The lattice spacing in the HRTEM image (Figure 7b) can be clearly seen with distances of 0.282 and 0.455 nm, corresponding to the (001) planes and (200) planes of $Na_{0.44}MnO_2$, respectively. The same structure of electrode discharged to 2.8 V with the original one is in accordance with the *in-suit* synchrtron XRD result, and further demonstrates the robust structure of NMO850. The corresponding SAED pattern (Figure 7c) indicates that the sample retains its single-crystalline nature in the [0-10] direction. The high stability of this robust multi-angular structure is crucial for the superior cycling performance of $Na_{0.44}MnO_2$.

4. CONCLUSION

In summary, we synthesized multi-angular rod-shaped $Na_{0.44}MnO_2$ via a reverse microemulsion method and studied the electrochemical performance as cathode materials for sodium-ion batteries. With the benefits of multi-angular morphology, suitable size, and fast sodium ion diffusion, the as-prepared $Na_{0.44}MnO_2$ rods prepared at 850°C as a cathode material for SIBs possess stable cycling performance with capacity of 72.8 mAh g^{-1} and capacity retention of 99.6% after 2000 cycles at 8.3 C. The as-designed multi-angular

$Na_{0.44}MnO_2$ provides new insight into the development of tunnel-type electrode materials and their application in rechargeable sodium-ion batteries.

ASSOCIATED CONTENT

Supporting Information

Schematic crystal structure of $Na_{0.44}MnO_2$. XRD and SEM images of powders. Electrochemical performance of NMO850 and NMO900. This material is available free of charge via the Internet at http://pubs.acs.org**.**

AUTHOR INFORMATION

Corresponding Author

E-mail addresses: shulei@uow.edu.au (Shulei Chou); ziqi.sun@qut.edu.au (Ziqi Sun); qinfen.gu@synchrotron.org.au

Acknowledgements

This work was partly supported by an Australian Research Council (ARC) Discovery Project (DP160102627). Q. Liu is supported by funding from the China Scholarship Council (No. 201406370169). The authors also thank Dr Tania Silver for critical reading of the manuscript, and acknowledge the use of the facilities in the UOW Electron Microscopy Centre, with special thanks for Dr. David Mitchell.

References

1. Dunn, B.; Kamath, H.; Tarascon, J.-M., Electrical Energy Storage for the Grid: a Battery of Choices. *Science* **2011,** *334* (6058), 928-935.

2. Palomares, V.; Serras, P.; Villaluenga, I.; Hueso, K. B.; Carretero-González, J.; Rojo, T., Na-ion batteries, Recent Advances and Present Challenges to Become Low Cost Energy Storage Systems. *Energy Environ. Sci.* **2012,** *5* (3), 5884-5901.

3. Dou, Y.; Xu, J.; Ruan, B.; Liu, Q.; Pan, Y.; Sun, Z.; Dou, S. X., Atomic Layer-by-Layer Co_3O_4/Graphene Composite for High Performance Lithium-Ion Batteries. *Adv. Energy Mater.* **2016**. DOI: 10.1002/aenm.201501835.

4. Hu, Z.; Zhu, Z.; Cheng, F.; Zhang, K.; Wang, J.; Chen, C.; Chen, J., Pyrite FeS_2 for High-Rate and Long-Life Rechargeable Sodium Batteries. *Energy Environ. Sci.* **2015,** *8* (4), 1309-1316.

5. Slater, M. D.; Kim, D.; Lee, E.; Johnson, C. S., Sodium-Ion Batteries. *Adv. Funct. Mater.* **2013,** *23* (8), 947-958.

6. Xiang, X.; Zhang, K.; Chen, J., Recent Advances and Prospects of Cathode Materials for Sodium-Ion Batteries. *Adv. Mater.* **2015,** *27* (36), 5343-5364.

7. Li, Y.; Hu, Y.-S.; Qi, X.; Rong, X.; Li, H.; Huang, X.; Chen, L., Advanced Sodium-Ion Batteries using Superior Low Cost Pyrolyzed Anthracite Anode: towards Practical Applications. *Energy Storage Mater.* **2016,** *5*, 191-197.

8. Mu, L.; Xu, S.; Li, Y.; Hu, Y. S.; Li, H.; Chen, L.; Huang, X., Prototype Sodium-Ion Batteries Using an Air-Stable and Co/Ni-Free O3-Layered Metal Oxide Cathode. *Adv. Mater.* **2015,** *27* (43), 6928-6933.

9. Parant, J.-P.; Olazcuaga, R.; Devalette, M.; Fouassier, C.; Hagenmuller, P., Sur Quelques Nouvelles Phases de Formule Na_xMnO_2 ($x \leqslant 1$). *J. Solid State Chem.* **1971,** *3* (1), 1-11.

10. Han, D. W.; Ku, J. H.; Kim, R. H.; Yun, D. J.; Lee, S. S.; Doo, S. G., Aluminum Manganese Oxides with Mixed Crystal Structure: High-Energy-Density Cathodes for Rechargeable Sodium Batteries. *ChemSusChem* **2014,** *7* (7), 1870-1875.

11. Li, Y.; Wu, Y., Formation of $Na_{0.44}MnO_2$ Nanowires via Stress-Induced Splitting of Birnessite Nanosheets. *Nano Res.* **2009,** *2* (1), 54-60.

12. Doeff, M. M.; Anapolsky, A.; Edman, L.; Richardson, T. J.; De Jonghe, L., A High-Rate Manganese Oxide for Rechargeable Lithium Battery Applications. *J. Electrochem. Soc.* **2001,** *148* (3), A230-A236.

13. Akimoto, J.; Hayakawa, H.; Kijima, N.; Awaka, J.; Funabiki, F. In Single-Crystal Synthesis and Structure Refinement of $Na_{0.44}MnO_2$, Solid State Phenomena, Trans Tech Publ: **2011**; pp 198-202.

14. Kim, D. J.; Ponraj, R.; Kannan, A. G.; Lee, H.-W.; Fathi, R.; Ruffo, R.; Mari, C. M.; Kim, D. K., Diffusion Behavior of Sodium Ions in $Na_{0.44}MnO_2$ in Aqueous and Non-aqueous Electrolytes. *J. Power Sources* **2013,** *244*, 758-763.

15. Zhou, X.; Guduru, R. K.; Mohanty, P., Synthesis and Characterization of $Na_{0.44}MnO_2$ from Solution Precursors. *J. Mater. Chem. A* **2013,** *1* (8), 2757-2761.
16. Zhan, P.; Wang, S.; Yuan, Y.; Jiao, K.; Jiao, S., Facile Synthesis of Nanorod-like Single Crystalline $Na_{0.44}MnO_2$ for High Performance Sodium-Ion Batteries. *J. Electrochem. Soc.* **2015,** *162* (6), A1028-A1032.
17. Doeff, M. M.; Peng, M. Y.; Ma, Y.; De Jonghe, L., Orthorhombic Na_xMnO_2 as a Cathode Material for Secondary Sodium and Lithium Polymer Batteries. *J. Electrochem. Soc.* **1994,** *141* (11), L145-L147.
18. Wang, Y.; Mu, L.; Liu, J.; Yang, Z.; Yu, X.; Gu, L.; Hu, Y. S.; Li, H.; Yang, X. Q.; Chen, L., A Novel High Capacity Positive Electrode Material with Tunnel-Type Structure for Aqueous Sodium-Ion Batteries. *Adv. Energy Mater.* **2015**. DOI: 10.1002/aenm.201501005.
19. Sauvage, F.; Laffont, L.; Tarascon, J.-M.; Baudrin, E., Study of the Insertion/deinsertion Mechanism of Sodium into $Na_{0.44}MnO_2$. *Inorg. Chem.* **2007,** *46* (8), 3289-3294.
20. Cao, Y.; Xiao, L.; Wang, W.; Choi, D.; Nie, Z.; Yu, J.; Saraf, L. V.; Yang, Z.; Liu, J., Reversible Sodium Ion Insertion in Single Crystalline Manganese Oxide Nanowires with Long Cycle Life. *Adv. Mater.* **2011,** *23* (28), 3155-3160.
21. Wang, Y.; Liu, J.; Lee, B.; Qiao, R.; Yang, Z.; Xu, S.; Yu, X.; Gu, L.; Hu, Y.-S.; Yang, W., Ti-Substituted Tunnel-Type $Na_{0.44}MnO_2$ Oxide as a Negative Electrode for Aqueous Sodium-Ion Batteries. *Nat. Commun.* **2015,** *6*. DOI:10.1038/ncomms7401.
22. Hosono, E.; Saito, T.; Hoshino, J.; Okubo, M.; Saito, Y.; Nishio-Hamane, D.; Kudo, T.; Zhou, H., High Power Na-Ion Rechargeable Battery with Single-Crystalline $Na_{0.44}MnO_2$ Nanowire Electrode. *J. Power Sources* **2012,** *217*, 43-46.
23. MingáLi, C., Synthesis and Application of Ultra-Long $Na_{0.44}MnO_2$ Submicron Slabs as a Cathode Material for Na-Ion Batteries. *RSC Adv.* **2014,** *4* (72), 38140-38143.
24. Lu, C.-H.; Wang, H.-C., Reverse-Microemulsion Preparation and Characterization of Ultrafine Orthorhombic $LiMnO_2$ Powders for Lithium-Ion Secondary Batteries. *J. Eur. Ceram. Soc.* **2004,** *24* (5), 717-723.
25. Lu, C.-H.; Yeh, P.-Y., Ultrafine Lithium Cobalt Oxide Powder Derived from A Water-in-Oil Emulsion Process. *J. Mater. Chem.* **2000,** *10* (3), 599-601.
26. Doeff, M. M.; Richardson, T. J.; Kepley, L., Lithium Insertion Processes of Orthorhombic Na_xMnO_2 ‐ Based Electrode Materials. *J. Electrochem. Soc.* **1996,** *143* (8), 2507-2516.
27. Liu, Q.; Sun, Z.; Dou, Y.; Kim, J. H.; Dou, S. X., Two-Step Self-Assembly of Hierarchically-Ordered Nanostructures. *J. Mater. Chem. A* **2015,** *3* (22), 11688-11699.
28. Tevar, A.; Whitacre, J., Relating Synthesis Conditions and Electrochemical Performance for the Sodium Intercalation Compound $Na_4Mn_9O_{18}$ in Aqueous Electrolyte. *J. Electrochem. Soc.* **2010,** *157* (7), A870-A875.

29. Hosono, E.; Matsuda, H.; Honma, I.; Fujihara, S.; Ichihara, M.; Zhou, H., Synthesis of Single Crystalline Electro-Conductive $Na_{0.44}MnO_2$ Nanowires with High Aspect Ratio for the Fast Charge–Discharge Li Ion Battery. *J. Power Sources* **2008,** *182* (1), 349-352.
30. Pang, G.; Nie, P.; Yuan, C.; Shen, L.; Zhang, X.; Zhu, J.; Ding, B., Enhanced Performance of Aqueous Sodium-Ion Batteries Using Electrodes Based on the $NaTi_2(PO_4)_3$/MWNTs–$Na_{0.44}MnO_2$ System. *Energy Technol.* **2014,** *2* (8), 705-712.
31. Sauvage, F.; Baudrin, E.; Tarascon, J.-M., Study of the Potentiometric Response towards Sodium Ions of $Na_{0.44-x}MnO_2$ for the Development of Selective Sodium Ion Sensors. *Sens. Actuators, B: Chem.* **2007,** *120* (2), 638-644.
32. Ju, J.; Bai, H.; Zheng, Y.; Zhao, T.; Fang, R.; Jiang, L., A Multi-Structural and Multi-Functional Integrated Fog Collection System in Cactus. *Nat. Commun.* **2012,** *3*, 1247.
33. Berthelot, R.; Carlier, D.; Delmas, C., Electrochemical Investigation of the P2–Na_xCoO_2 Phase Diagram. *Nat. Mater.* **2011,** *10* (1), 74-80.
34. Li, Z.; Young, D.; Xiang, K.; Carter, W. C.; Chiang, Y. M., Towards High Power High Energy Aqueous Sodium-Ion Batteries: the $NaTi_2(PO_4)_3$/$Na_{0.44}MnO_2$ System. *Adv. Energy Mater.* **2013,** *3* (3), 290-294.
35. Zhang, X.-H.; Pang, W.-L.; Wan, F.; Guo, J.-Z.; Lü, H.-Y.; Li, J.-Y.; Xing, Y.-M.; Zhang, J.-P.; Wu, X.-L., P2–$Na_{2/3}Ni_{1/3}Mn_{5/9}Al_{1/9}O_2$ Microparticles as Superior Cathode Material for Sodium-Ion Batteries: Enhanced Properties and Mechanisam via Graphene Connection. *ACS Appl. Mater. Interfaces* **2016,** *8* (32), 20650-20659.
36. Xu, S.; Wang, Y.; Ben, L.; Lyu, Y.; Song, N.; Yang, Z.; Li, Y.; Mu, L.; Yang, H. T.; Gu, L., Fe-Based Tunnel-Type $Na_{0.61}[Mn_{0.27}Fe_{0.34}Ti_{0.39}]O_2$ Designed by a New Strategy as a Cathode Material for Sodium-Ion Batteries. *Adv. Energy Mater.* **2015,** *5* (22). DOI: 10.1002/aenm.201501156.

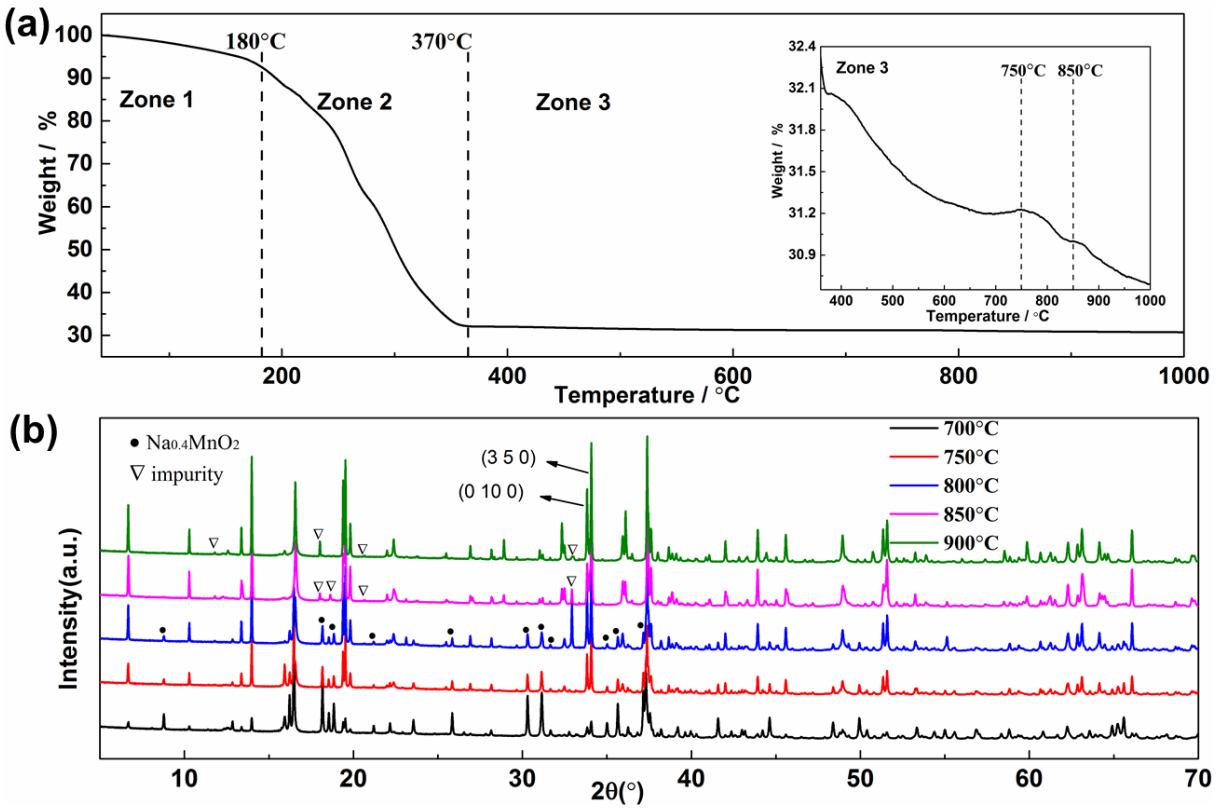

Figure 1. (a) TGA curve of the gel precursor between 40 – 1000°C with a ramp rate of 5°C min^{-1} (inset is an enlargement of Zone 3); (b) synchrotron powder XRD spectra of samples calcined at different temperatures. The 2θ angle has been converted to values corresponding to the more common laboratory Cu K_α radiation.

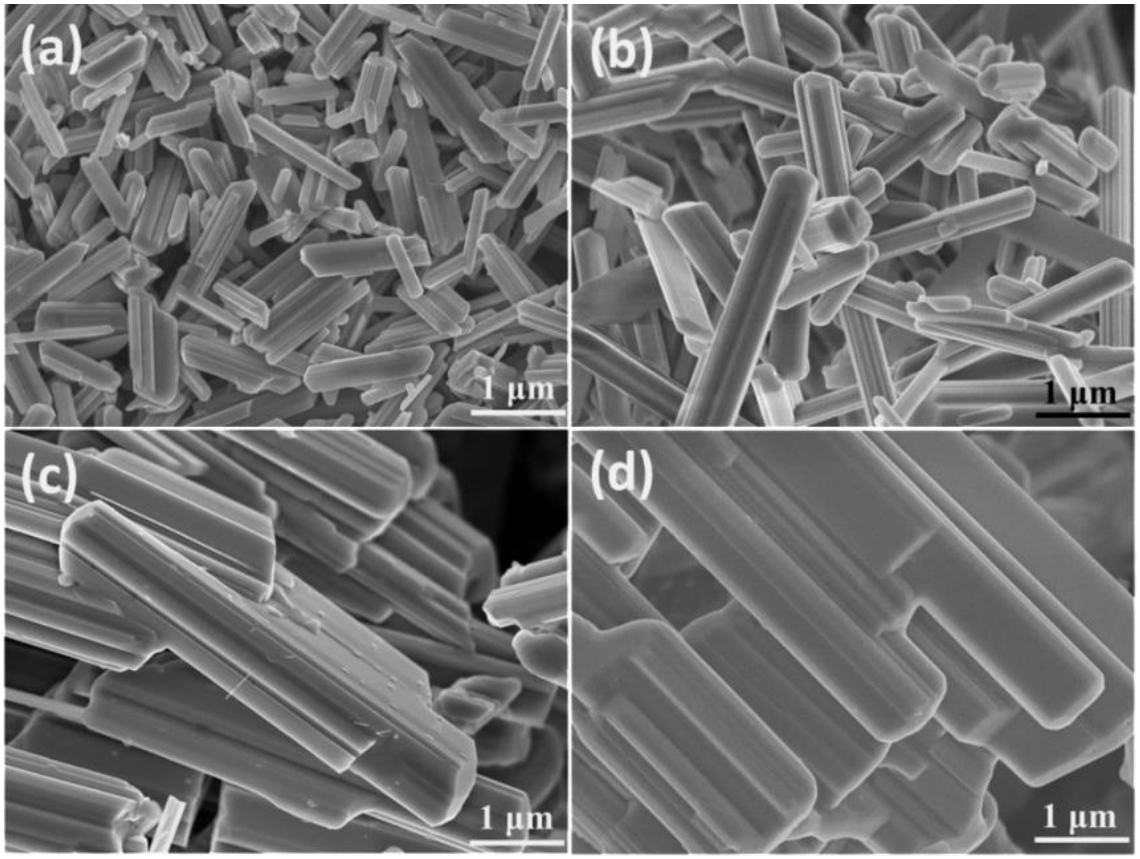

Figure 2. SEM morphologies of samples calcined at (a) 750°C; (b) 800°C; (c) 850°C; and (d) 900°C.

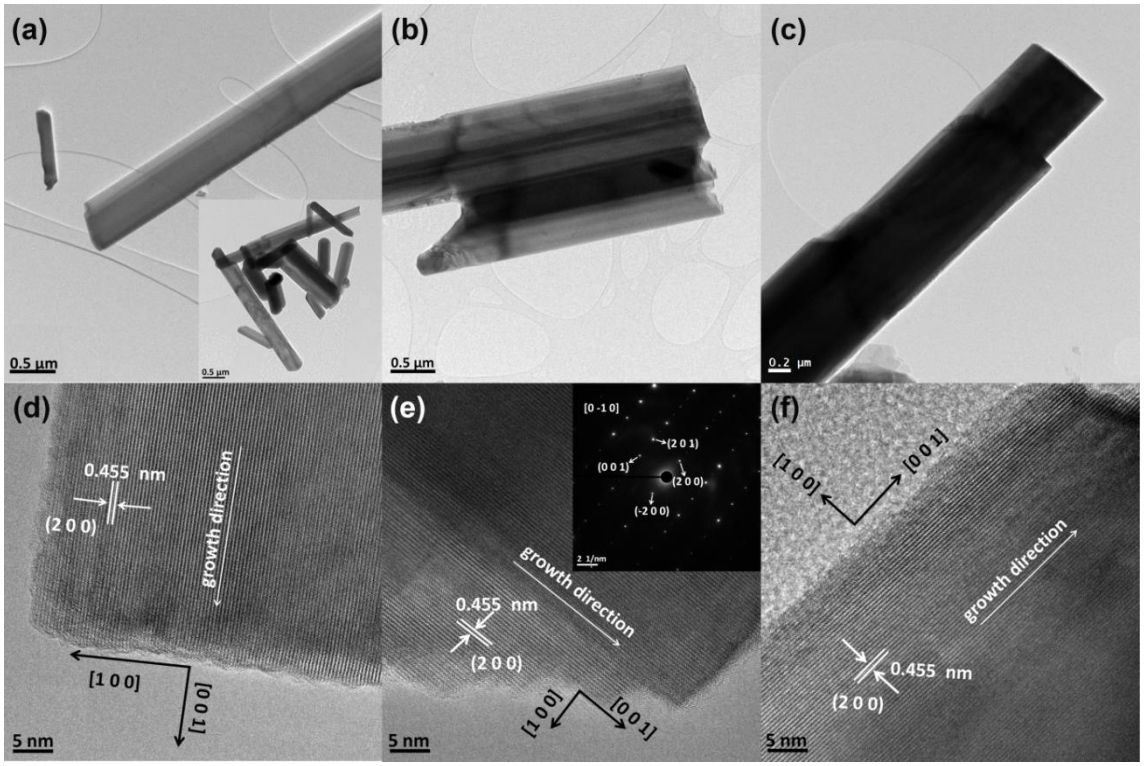

Figure 3. TEM images of samples calcined at (a) 800°C (inset: lower magnification); (b) 850°C; and (c) 900°C; HRTEM images of samples calcined at (d) 800°C; (e) 850°C (inset: corresponding SAED pattern); and (f) 900°C.

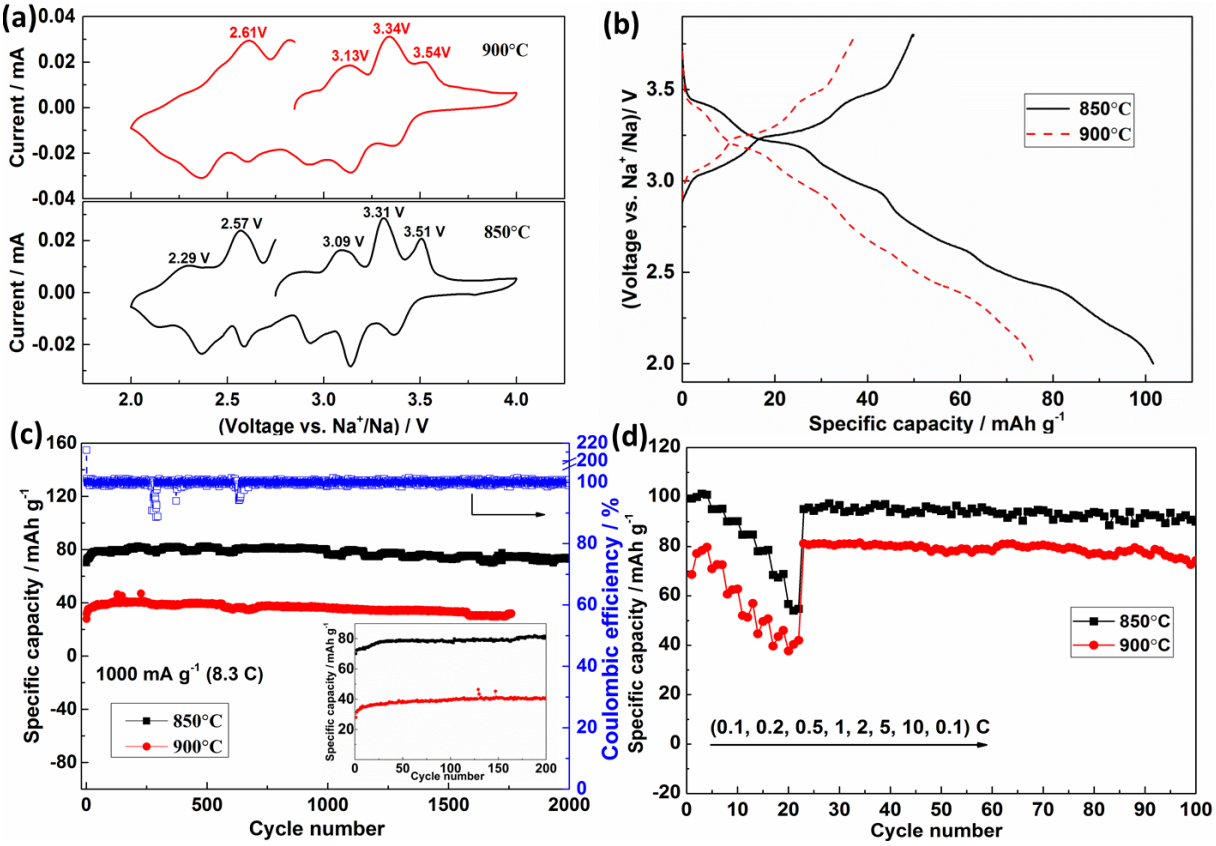

Figure 4. Electrochemical performances of NMO850 and NMO900: (a) cyclic voltammograms (CV) between 4.0-2.0 V; (b) charge-discharge profiles at 0.1 C; (c) cycling performance and coulombic efficiency of NMO850 and cycling performance of NMO900 at 8.3 C (inset: amplication image up to 200 cycles); and (d) rate capacity between 3.8-2.0 V.

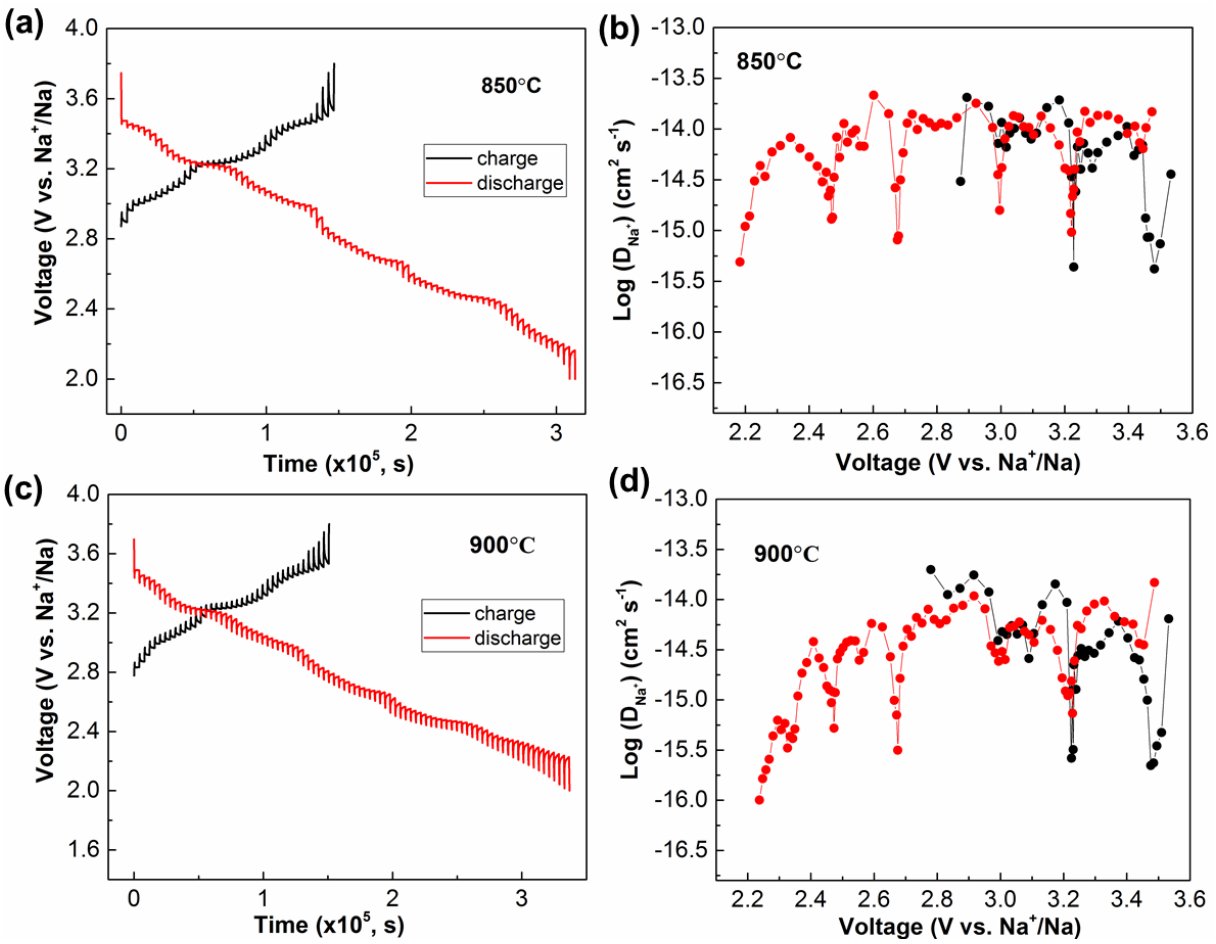

Figure 5. (a) GITT curves for the charge and discharge states of the 1st cycle and (b) corresponding sodium ion diffusion coefficent (D_{Na+}) for Na/NMO850 cell cycling at 0.1 C between 3.8-2.0 V; (c) GITT curves for the charge and discharge states of the 1st cycle and (d) corresponding D_{Na+} of Na/NMO900 cell cycling at 0.1 C between 3.8-2.0 V.

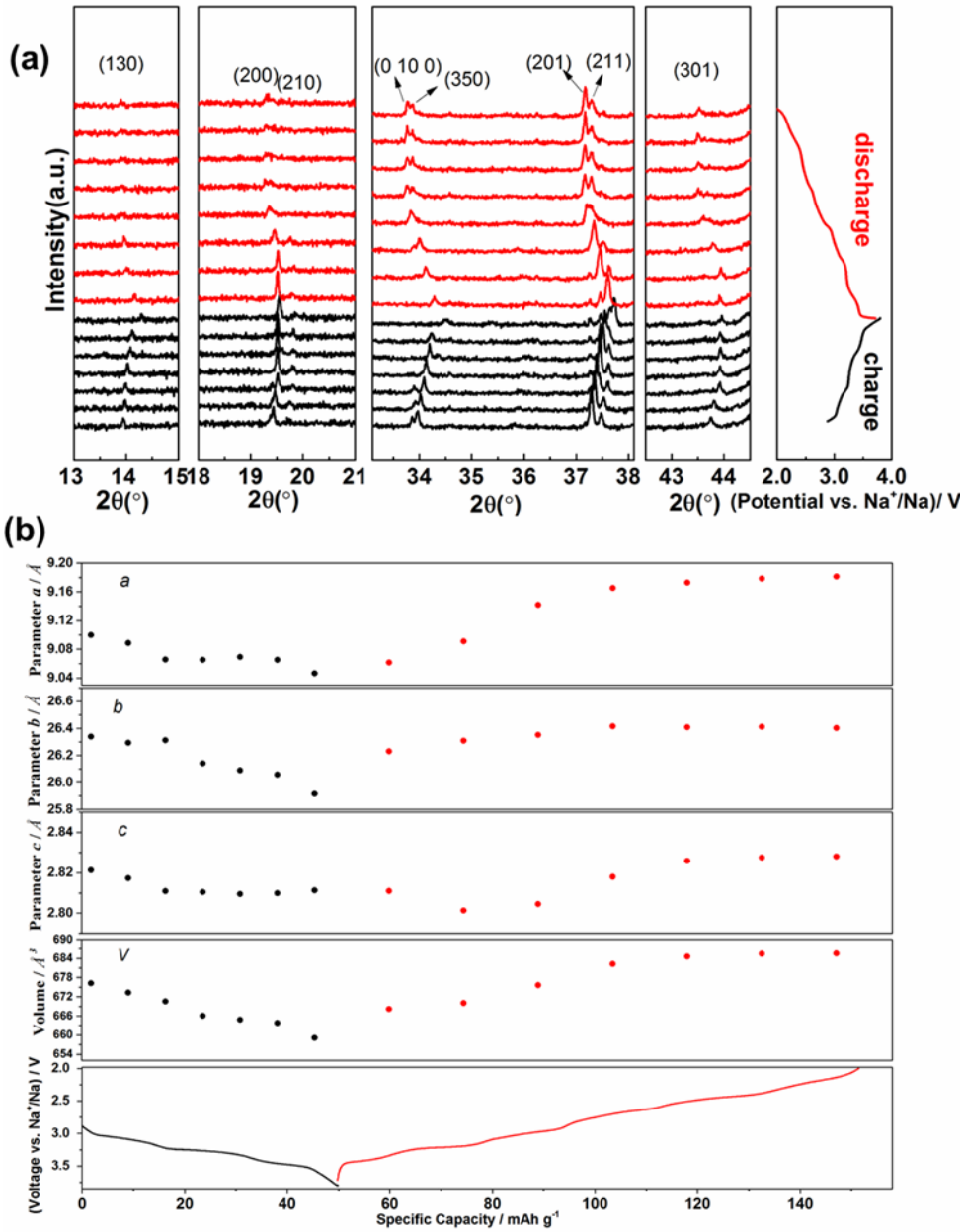

Figure 6. (a) *In situ* X-ray synchrotron diffraction patterns collected at 0.5 C between 3.8-2.0 V during the first charge/discharge process forNMO850; (b) corresponding changes of cell parameters *a*, *b*, and *c*, and the unit cell volume. The 2θ angle has been converted to values corresponding to the more common laboratory Cu K_α radiation.

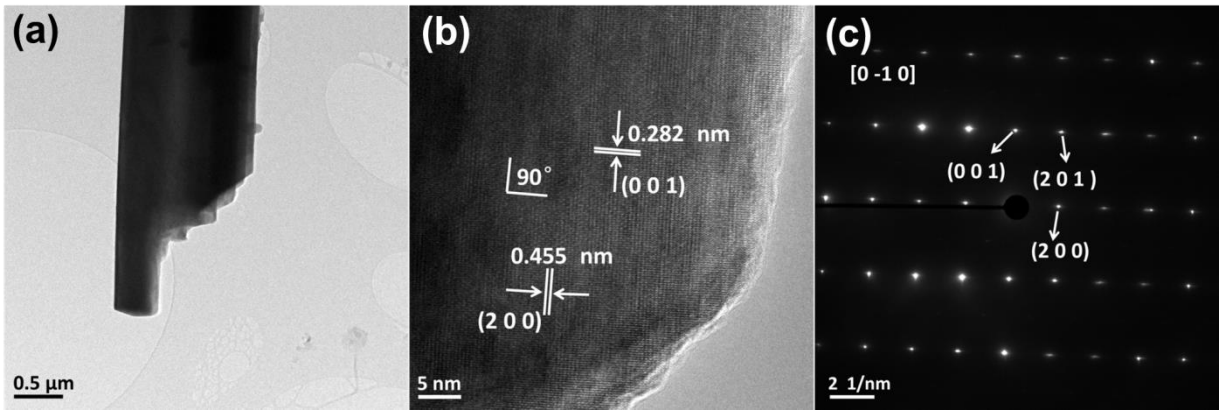

Figure 7. (a) TEM image, (b) HRTEM image, and (c) SAED pattern of NMO850 after cycling for 100 cycles at 0.1 C.

Table 1. Summary of $Na_{0.44}MnO_2$ prepared by different methods as sodium-ion battery cathodes.

Method	Calcination temperature, time	Morphology	Voltage (V vs. Na^+/Na)	Current density (rate)	Specific capacity/cycles
Pechini method [14]	800°C for 9 h	rod	2.0 – 3.8 V	0.1 C 1 C	65 mAh g^{-1} 32 mAh g^{-1}
Sol-gel method [23]	450°C for 6 h; 900°C for 15 h	slab	2.0 – 4.0 V	0.1C	~ 110 mAh g^{-1}/100
Hydrothermal method [22]	205°C for 96 h	nanowire	2.0 – 4.0 V	8.3 C	~ 90 mAh g^{-1}/20
Solid state method [19]	300°C for 8 h; 800°C for 9 h	rod	2.0 – 3.8 V	0.1 C	~ 40 mAh g^{-1}/45 for $Na_{0.44}MnO_2$/C electrode
Polymer-pyrolysis method [20]	750°C for 24 h	nanowire	2.0 – 4.0 V	0.5 C 2 C	84.2 mAh g^{-1}/1000 82 mAh g^{-1}
Reverse microemulsion method [16]	750°C for 24 h	rod	2.0 – 3.8 V	0.83 C	80.2 mAh g^{-1}/50
Our work	850°C for 20 h	multi-angular rod	2.0 – 3.8 V	0.1 C 8.3 C	99.1 mAh g^{-1}/100 82.1 mAh g^{-1}/1000

Table of Contents